Non-local Andreev reflection through Andreev molecular states in graphene Josephson junctions

2D Materials

OPEN ACCESS

RECEIVED
30 August 2022

REVISED
12 April 2023

ACCEPTED FOR PUBLICATION
19 April 2023

PUBLISHED
2 May 2023

MADE OPEN ACCESS
17 May 2023

PAPER

Non-local Andreev reflection through Andreev molecular states in graphene Josephson junctions

Eduárd Zsurka[1,*], **Noel Plaszkó**[1], **Péter Rakyta**[1,2] **and Andor Kormányos**[1,*]

[1] Department of Physics of Complex Systems, Eötvös Loránd University, Budapest, Hungary
[2] Wigner Research Center for Physics, 29-33 Konkoly-Thege Miklos Str., H-1121 Budapest, Hungary
[*] Authors to whom any correspondence should be addressed.

E-mail: eduard.zsurka@ttk.elte.hu and andor.kormanyos@ttk.elte.hu

Keywords: nonlocal Andreev reflection, graphene Josephson junction, Andreev molecular state

Supplementary material for this article is available online

Abstract

We propose that a device composed of two vertically stacked monolayer graphene Josephson junctions can be used for Cooper pair splitting. The hybridization of the Andreev bound states of the two Josephson junction can facilitate non-local transport in this normal-superconductor hybrid structure, which we study by calculating the non-local differential conductance. Assuming that one of the graphene layers is electron and the other is hole doped, we find that the non-local Andreev reflection can dominate the differential conductance of the system. Our setup does not require the precise control of junction length, doping, or super conducting phase difference, which could be an important advantage for experimental realization.

Quantum entangled particles have numerous potential applications in fields such as quantum communications or quantum cryptography. Thus, practical schemes of producing entangled particles are of fundamental interest [1]. One of the most promising candidates for creating entangled electron states is based on spin singlet Cooper pairs. It was proposed that if the electrons of a Cooper pair can be extracted coherently and separated spatially, they can serve as a source of entangled electrons [2, 3]. This process is known as Cooper pair splitting (CPS). As discussed in, e.g. [4, 5], the key physical process to achieve CPS is the non-local or crossed Andreev reflection (CAR).

Although the first observations of CPS were made in metallic nanostructures [6, 7], devices that use two quantum dots (QDs) have garnered the most attention in this field. The charging energy on the QDs prohibits the double occupancy on each dot, leading to the suppression of electron cotunneling (EC). EC is a competing process with CAR and it should be suppressed in order to achieve CPS. Experimentally CPS has been achieved in QD devices realized in InAs and InSb nanowires [8–13], carbon nanotubes [14, 15], graphene based QDs [16–18], and recently in 2DEGs [19]. Alongside the experimental effort, substantial theoretical work has also been devoted to the study of CPS in QD based devices [2, 3, 20–22].

A different approach to suppress EC with respect to CAR makes use of features in the density of states of semiconductors [23, 24]. Since this approach does not necessitate QDs, it should make the fabrication of CPS devices simpler. Regarding monolayer graphene, [23] predicted that pure CAR could be achieved in a n-type graphene−superconductor−p-type graphene junction, if the doping of the graphene is smaller than the superconductor pair potential Δ_0. In this case, the vanishing density of state of graphene at the Dirac point allows the elimination of processes that suppress CAR. However, due to the charge fluctuations around the Dirac point, which are usually larger [25, 26] than the value of Δ_0 of most superconductors, such a low doping is difficult to achieve experimentally. The problem of charge fluctuations can be mitigated, to some extent, by using bilayer graphene [27], because the larger density of states allows a better control of residual doping levels [27, 28]. Recently, the signatures of CPS have also been observed in multi-terminal ballistic graphene-superconductor structures [29]. Another

recent theoretical proposal [30, 31] suggested that the CAR probability can be enhanced in a device where the central region consists of two, coupled one-dimensional superconductors and two normal leads are attached on each side to one of the superconductors. The central region effectively constitutes a superconducting QD. The CAR can be resonantly enhanced by tuning the superconducting phase difference between the one-dimensional superconductors to $\phi \approx \pi$ and then adjusting the chemical potential of the superconductors.

In this work we propose that an approach based on Andreev molecular states (AMSs) [32, 33] can also help to achieve CAR dominated transport. It was suggested that Andreev bound states (ABSs) in closely spaced Josephson junctions (JJs) can overlap and hybridize forming AMSs. We study the possibility of CPS in a setup that harbors AMSs. The device consists of two graphene JJs displaced vertically with respect to each other, (see figure 1) such that the ABSs in the two junctions can hybridize. This type of graphene JJ has recently been studied experimentally in [34], focusing on superconducting interference device type operation and quantum Hall physics. We calculate the non-local, non-equilibrium differential conductance through the device, when two normal leads are weakly connected to the graphene layers, as shown in figure 1. Our most important finding is that CAR can be larger than EC even if the doping of the graphene layers is significantly larger than the value of Δ_0. Therefore, the CAR should be less affected by charge puddles, which are present in graphene at low doping.

1. The model

The schematics of the proposed four-terminal device is shown in figure 1. Two graphene monolayers (red and blue) of length L are placed above each other. They are separated by an insulator such as hBN or vacuum in the center of the device, i.e. for $0 < x < L$, meaning that there is no direct electrical contact between these two layers vertically. Two superconducting leads, S_L and S_R (dark gray) are attached to the edges of the top and bottom graphene layers, at $x = 0$ and $x = L$. In addition, two normal leads (light gray) N_1 and N_2 are weakly coupled to the middle ($x = L/2$) of the top and the bottom graphene layer, respectively. We note that a similar layout for a single graphene JJ junction was used in [35] to determine the energy spectrum of ABSs.

In our calculations the description of both the normal and the superconducting regions is based on the nearest-neighbor tight-binding model of graphene with in-plane hopping amplitude γ_0. The top and bottom graphene layers and the superconducting leads constitute the central region of the device, described by the Hamiltonian

$$H_C = \begin{pmatrix} H_{gr} - \mu_t & 0 & W_{NS} \\ 0 & H_{gr} - \mu_b & W_{NS} \\ W_{NS}^\dagger & W_{NS}^\dagger & H_S - \mu_S \end{pmatrix}. \quad (1)$$

Here H_{gr} is the Hamiltonian of undoped monolayer graphene, $H_S = \begin{pmatrix} H_{S_L} & 0 \\ 0 & H_{S_R} \end{pmatrix}$ is the Hamiltonian of the superconducting leads in the non-superconducting state. The leads S_L and S_R are modeled with Bernal stacked multilayer graphene, with out-of plane hopping amplitude γ_1. We assume that the top and bottom graphene layers are perfectly aligned and denote the doping by μ_t [μ_b] in the top [bottom] layer, while μ_S is the doping in S_L and S_R. W_{NS} describes the coupling between the graphene layers and the superconducting leads with hopping amplitude $\gamma_{NS} = \gamma_0$, corresponding to a perfectly transparent interface.

Before superconductivity is introduced, the total Hamiltonian of the system reads

$$H_{tot} = \begin{pmatrix} H_C & W_1 & W_2 \\ W_1^\dagger & H_1 & 0 \\ W_2^\dagger & 0 & H_2 \end{pmatrix}, \quad (2)$$

where $H_l = H_{gr} - \mu_l$ is the Hamiltonian of the normal leads N_l, with $l = 1, 2$. The leads N_l are also modelled by monolayer graphene and their doping is kept fixed at $\mu_l = 0.1$ eV. We checked that the results discussed below do not strongly depend on μ_l. W_l describes the coupling between N_l and the corresponding graphene layer (see figure 1).

To describe the transport properties of this system when the leads S_L and S_R are superconducting, we used the approach based on the Bogoliubov-de Gennes Hamiltonian. This can be compactly written as

$$\begin{pmatrix} H_{\text{tot}} - E_F & \tilde{\Delta}(x) \\ \tilde{\Delta}^*(x) & -H_{\text{tot}} + E_F \end{pmatrix} \begin{pmatrix} \Psi_e \\ \Psi_h \end{pmatrix} = \varepsilon \begin{pmatrix} \Psi_e \\ \Psi_h \end{pmatrix}, \quad (3)$$

where E_F is the Fermi energy, $\varepsilon > 0$ is the excitation energy, Ψ_e and Ψ_h are electron and hole wave functions, respectively. $\tilde{\Delta}(x)$ is a matrix which only has non-zero elements between degrees of freedom that belong to either S_L or S_R. To describe superconductivity, an s-wave pairing potential is used, which is nonzero only in the superconducting leads and changes in a step-function manner at the normal-superconducting interface: $\Delta(x) = \Delta_0[\theta(-x) + \theta(x - L)\exp(i\varphi)]$, where θ is the Heaviside function, and φ is the superconducting phase difference between S_L and S_R. The step-function change of the pair-potential at the boundary is valid if $\lambda_F^{(S)} \ll \lambda_F^{(t,b)}, \xi_0$ [36]. Here $\lambda_F^{(S)}$ and $\lambda_F^{(t,b)}$ are the Fermi wavelength in the superconducting leads and central graphene layers and $\xi_0 = \hbar v_F/\Delta_0$ is the (in-plane) ballistic superconducting coherence length,

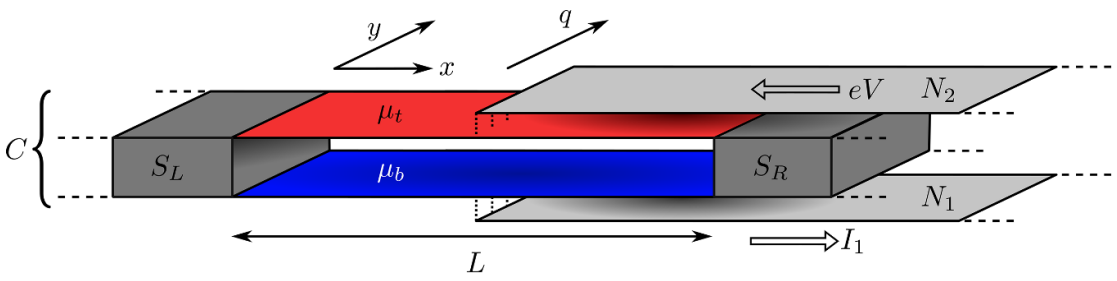

Figure 1. A schematic of the device. Two graphene monolayers (red and blue) of length L and doping μ_t and μ_b are placed above each other and are connected at either side to superconducting leads S_L and S_R (dark gray). Normal leads N_1 and N_2 (light gray) are connected to each graphene layer at $x = L/2$. Translation invariance in the y direction is assumed. To study the properties of the device, we calculate the dependence of the current I_1 in N_1, when a voltage V is applied to N_2.

$v_F \approx 10^6$ m s^{-1} being the Fermi velocity of monolayer graphene. We use highly doped superconducting leads with $\mu_S = 0.8$ eV, therefore the above condition is satisfied in all our calculations. Since the in-plane γ_0 and out-of plane γ_1 hopping amplitudes in Bernal stacked multilayer graphene are different, it is intuitive to define an effective superconducting coherence length $\xi_\perp \neq \xi_0$ associated with the out-of-plane hopping in the superconducting leads. One can expect that interlayer Andreev reflection from the top to the bottom graphene layers is only significant if $d \lesssim \xi_\perp$, where d is the vertical distance between these layers. We explain how $\xi_\perp$ is estimated in Supplementary Information (SI), here we only mention than in all subsequent calculations $d \ll \xi_\perp$.

In the transport calculations we assume that a voltage V is applied (with respect to E_F) to the top normal lead N_2 and the current I_1 is measured in the bottom normal lead N_1, as shown in figure 1. We calculate the non-local differential conductance $G(eV) = \mathrm{d}I_1/\mathrm{d}V$ which depends on CAR. We are primarily interested in the case of wide graphene layers, where exact termination of the edges does not matter because the transport properties are determined by bulk states. Using hard wall boundary conditions [37, 38], the transverse wavenumber q parallel to the y direction is a good quantum number, see the SI for further details. The numerical calculations discussed below were performed using the tight-binding framework implemented in the EQuUs [39] package.

2. Andreev molecular states

The Andreev reflection of quasiparticles at the graphene-superconductor interfaces leads to the formation of correlated electron–hole states known as ABSs [35, 36, 40–43], with energies $E_n \leqslant \Delta_0$. Their presence in the proximitized graphene layers means that an induced gap Δ_{ind} appears in the graphene layers, which is smaller than the pairing potential Δ_0 of the superconductors. If the superconducting phase difference φ is fixed, in ballistic systems the magnitude of Δ_{ind} is determined by the smaller of two energy scales, namely, the bulk gap Δ_0 and the Thouless energy $E_{Th} = \hbar v_F/L$.

For $\varphi = 0$, when $E_{Th} \gg \Delta_0$, i.e. in the short junction regime $\Delta_{ind} \cong \Delta_0$. In the opposite case $E_{Th} \ll \Delta_0$, the dominant energy scale is E_{Th}; this is the long junction regime where Δ_{ind} is considerably smaller than Δ_0. Note that the ratio of E_{Th} and Δ_0 can also be expressed as $E_{Th}/\Delta_0 = \xi_0/L$, so that the short junction regime corresponds $E_{Th}/\Delta_0 \gg 1$. In this work, we study devices with Thouless energy between $0.4\Delta_0$ and $3\Delta_0$. Junctions with E_{Th} in this range correspond to the intermediate length regime, where analytic results valid in the short [36] or long [40] regime of a JJ consisting of a single graphene layer do not strictly apply. Taking $\Delta_0 = 1$ meV, the aforementioned E_{Th} values correspond to L between 210 and 1580 nm.

One can expect that in the setup shown in figure 1, the ABSs formed in the two graphene layers can hybridize, leading to the formation of AMSs [32, 33]. In order to see the effects of ABS hybridization, we start by considering the properties of ABSs formed in individual layers, i.e. when one of the graphene layers, e.g. the bottom one is disconnected from the superconductors and only the top one is connected. We also disconnect the lead N_2 and calculate the Green's function of the resulting graphene JJ. The spectrum of the ABSs is determined performing local density of states (LDOS) calculations for energies $0 \leqslant E \leqslant \Delta_0$. The LDOS is calculated as the sum of the LDOS of electron and hole type quasiparticles $\rho(E,q) = \rho^e(E,q) + \rho^h(E,q) = -(1/\pi)\mathrm{Im}(\mathrm{G}^R)$, where $\mathrm{Im}(\mathrm{G}^R)$ is the imaginary part of the retarded Green's function. The LDOS is evaluated on ~ 10 unit cells of the top layer around $x = L/2$. In figures 2(a)–(c) we show results for superconducting phase differences $\varphi = 0, \pi/2$ and π, using $\mu_t = -5$ meV and $E_{Th} = \Delta_0$. One can clearly see the appearance of multiple ABSs. Above $E = 0$ there is an energy range where no ABSs are present indicating the induced gap Δ_{ind}. One can observe that as φ increases from 0 to π, the induced gap Δ_{ind} decreases and at $\varphi = \pi$ the induced gap is closed. This can be shown analytically in both the short [36] and long [40] junction regime and also agrees with the experimental results of [35].

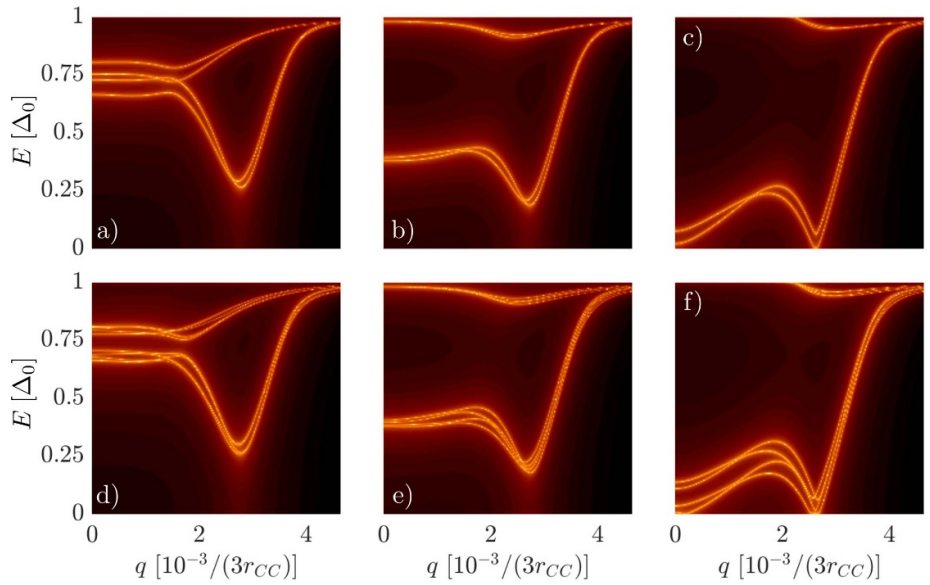

Figure 2. Local density of state calculations of ABSs as a function of the momentum q, for three different superconducting phase differences φ. (a)–(c) LDOS of ABSs in a monolayer graphene JJ, for $\varphi = 0, \pi/2$ and π going from left to right. (d)–(f) LDOS of AMS in the top graphene layer, i.e. when both graphene layers are connected to the superconductors, for $\varphi = 0, \pi/2$ and π going from left to right. We used doping $\mu_b = -\mu_t = 5\Delta_0$ and $E_{Th} = \Delta_0$ in all cases.

Turning now to the bilayer setup of figure 1, the distance between the graphene layers is taken to be $d = 3.3$ nm in our calculations, while we found that $\xi_\perp \approx 38$ nm (see SI). Since $d \ll \xi_\perp$, the coupling between the ABSs can lead to the formation of AMSs [32, 33]. This is shown in figures 2(d)–(f), where one can see the LDOS $\rho_t(E, q)$ calculated in the top graphene layer. At this stage the normal leads N_1 and N_2 are not yet connected to the graphene layers. For AMSs with energies $E_n \lesssim \Delta_0$ the relatively weak hybridization leads to only minor modifications of the LDOS, cf figures 2(a)–(c). However, for $\varphi = \pi$ there are AMSs with energy $E_n \gtrsim 0$ which are more strongly modified by interlayer hybridization (figure 2(f)). One can also see that, similarly to the case of ABSs (figures 2(a)–(c)), the magnitude of Δ_{ind} in the presence of AMSs can be tuned by changing φ (figures 2(d)–(f)).

One can expect that in order to have a finite interlayer transmission of electrons from N_1 to N_2 in the bias window $|eV| \leqslant \Delta_0$, Δ_{ind} has to be smaller than Δ_0. Therefore, Δ_{ind} is an important parameter of the device. We calculated Δ_{ind} as a function of the doping μ and E_{Th}, where $\mu = \mu_b = -\mu_t$, see figure 3. The value of Δ_{ind} is extracted from LDOS calculations by determining the minimum of the AMS spectrum. We find that for $\varphi = 0$ and $E_{Th} = 0.4\Delta_0, 0.6\Delta_0$ the induced gap is suppressed $\Delta_{ind} \ll \Delta_0$ (figure 3(a)). However, for larger values of $E_{Th} = 0.8\Delta_0 - 3\Delta_0$ a general observation is that Δ_{ind} is comparable to Δ_0 for low doping, but increasing μ leads to the reduction of Δ_{ind}. For large enough doping the induced gap can be suppressed regardless of the Thouless energy

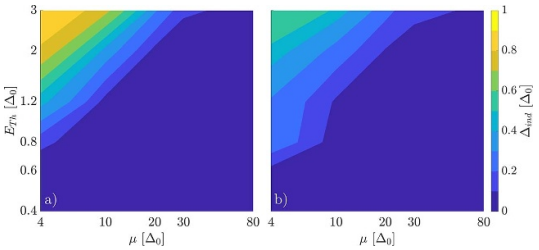

Figure 3. Size of the induced gap Δ_{ind} (in units of Δ_0) as a function of the magnitude of the doping μ, where $\mu = \mu_b = -\mu_t$, and Thouless energy E_{Th}, for superconducting phase difference (a) $\varphi = 0$ and (b) $\varphi = \pi/2$.

for the E_{Th} values we studied. In short, the condition $\Delta_{ind} < \Delta_0$ is satisfied for a wide range of (μ, E_{Th}) values. Note that tuning the doping changes not only Δ_{ind}, but also the number of the AMSs. Furthermore, as illustrated in figures 2(d)–(f), by increasing φ the AMSs are shifted deeper into superconducting gap and Δ_{ind} decreases (figure 3(b)). We find that in these ballistic devices for $\varphi = \pi$ the induced gap disappears regardless of the value of E_{Th}.

3. Differential conductance

We now discuss the transport through the central region of the device when the normal leads N_1 and N_2 are attached, as shown in figure 1. We are interested in the dependence of I_1 in N_1 on the applied voltage V to N_2. We restrict our study to voltages $|eV| \leqslant \Delta_0$,

therefore one expects that the transport is mediated by the AMSs in the junction. We use the Keldysh non-equilibrium Green's function technique [44–48] to calculate $dI_1/dV = G(eV,q)$ for a given q and then sum the contributions of the different q values, see the SI for more details. The differential conductance is given by

$$G(eV,q) = -\frac{2e}{h}\mathrm{Re}\left\{\frac{d}{dV}\int dE\mathrm{Tr}\left[\tau_z W_1 \mathrm{G}^{<}_{C,1}(E,eV)\right]\right\}, \tag{4}$$

where τ_z is a Pauli matrix acting in the electron–hole space and $\mathrm{G}^{<}_{C,1}(E,eV)$ is the bottom lead–central region lesser Green's function. To lighten the notations, the q dependence of $\mathrm{G}^{<}_{C,1}(E,eV)$ is not written explicitly. The differential conductance $G(eV)$ can be evaluated as

$$G(eV) = \sum_q G(eV,q) = \frac{w}{2\pi}\int G(eV,q)\,dq, \tag{5}$$

where w is the width of the junction in the y direction. All calculations are performed at $T = 0$ K temperature.

In order to obtain an insight into the transport properties of this setup, let us first consider a simple model: we assume that only a single AMS of energy E_{AMS} is present, which extends over both graphene layers in the central region. We neglect the q dependence of the AMS and assume that coupling between N_1 (N_2) and bottom (top) graphene layers is weak. According to the calculations detailed in the SI, the differential conductance can be approximated by

$$G(eV) \approx \frac{4e}{h}\frac{(\Gamma^e_1-\Gamma^h_1)(\Gamma^e_2-\Gamma^h_2)}{(eV-E_{\mathrm{AMS}})^2+\Gamma^2}, \tag{6}$$

where Γ^{α}_l are level broadenings [49] due to the coupling of the electron [hole] ($\alpha = e[h]$) part of the AMS to the states in N_l at energy E_{AMS}, and $\Gamma = \Gamma^e_1 + \Gamma^h_1 + \Gamma^e_2 + \Gamma^h_2$. Equation (6) shows that the presence of an AMS results in a resonant peak of Lorentzian lineshape in the differential conductance, at $eV \approx E_{\mathrm{AMS}}$. The signature of CAR dominated transport is $G(eV) < 0$, meaning that an injected electron in N_2 is transmitted as a hole into N_1. The sign of $G(eV)$ is determined by the numerator in equation (6), which depends on the difference between the level broadening of electron- and hole-like degrees of freedom of the AMS.

In the tunneling limit $\Gamma^{e(h)}_l$ depends on the product of the LDOS of the electron (hole) component of the AMS and of the attached leads N_l. Since the leads are metalic, their LDOS is constant. Therefore $\Gamma^e_l - \Gamma^h_l$ depends mainly on the difference of the LDOS of the electron and hole type quasiparticles in the AMS. One can expect that this can be changed by two means: firstly, by tuning the doping of the two graphene layers. Secondly, since the AMS wave functions depend on the superconducting phase difference φ, the LDOS can also be changed by tuning φ. Thus, this simple model suggests that one has two experimental knobs to tune the interlayer transmission and try to achieve CAR dominated transport.

As it can be seen in figure 2, for finite doping of the graphene layers, multiple AMS are present in our setup. The result given in equation (6) can be easily generalized to this case (see the SI). One finds that $G(eV,q)$ defined in equation (4) reads

$$G(eV,q) = \frac{4e^2}{h}\sum_{m,n}\frac{(\Gamma^e_{1,mn}(q)-\Gamma^h_{1,mn}(q))(\Gamma^e_{2,mn}(q)-\Gamma^h_{2,mn}(q))}{(eV-E_m(q)+i\Gamma_{mm}(q))(eV-E_n(q)-i\Gamma_{nn}(q))}, \tag{7}$$

where the summation runs over the number of the AMSs, Γ_{nm} depends on the product of the wave functions of the nth and mth AMS and $\Gamma_{nn} = \sum_{l,\alpha}\Gamma^{\alpha}_{l,nn}$. The $m = n$ terms are Lorentzian resonances, this is the type of contribution we have already discussed when we derived equation (6). The $m \neq n$ terms correspond to a 'cross-talk' between different AMSs and they are affected by interference effects between different AMSs. Therefore, in general, $G(eV,q)$ depends both on the LDOS and on the interference of the quasiparticle components of the AMSs.

Note, that in [23, 24] the enhancement of the probability of CAR is related to the DOS of the semiconducting leads, which are attached to a central superconducting strip, and their different doping. In our setup the leads N_l are assumed to be metallic and their doping does not play an important role. Moreover, as we discussed above, in our case quasiparticle interference also affects $G(eV)$, but as we will show in section 4 it does not lead to the type of resonant enhancement of CAR as in [30, 31]. These considerations clearly show the difference between our proposal and those of [23, 24, 30, 31].

4. Negative non-local Andreev reflection

We start with calculations which illustrate the complex interplay of LDOS and interference related effects in the differential conductance. In figure 4 we show the LDOS difference of the electron and hole quasiparticles of AMSs $\delta\rho_t(E,q) = \rho^e_t(E,q) - \rho^h_t(E,q)$ ($\delta\rho_b(E,q) = \rho^e_b(E,q) - \rho^h_b(E,q)$) in the top (bottom) graphene layers. These results were obtained in the same way as the total LDOS $\rho(E,q)$ in figures 2(d)–(f), i.e. evaluated on ~ 10 unit cells around $x = L/2$. We consider two cases: $\mu_b = -\mu_t$ (asymmetric doping) and $\mu_b = \mu_t$ (symmetric doping) and the parameters of the calculations correspond to the case shown in figure 2(d). In a given layer the sign

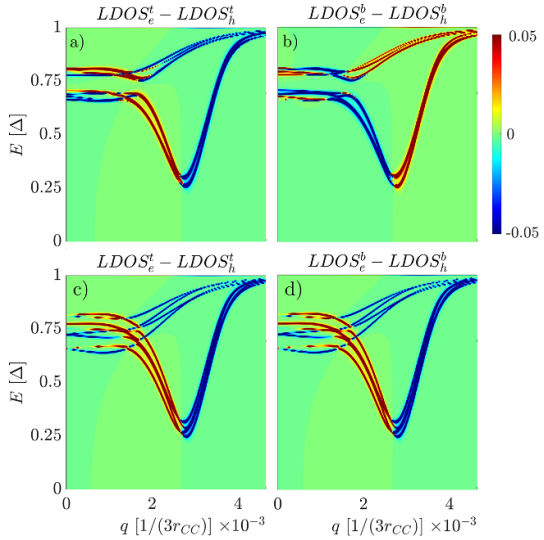

Figure 4. The LDOS difference of the electron and hole quasiparticles of AMSs in the top and bottom graphene layers. (a) $\delta\rho_t(E,q)$ and (b) $\delta\rho_b(E,q)$ for asymmetric doping and (c) and (d) for symmetric doping, respectively. Here $\varphi = 0$, $E_{Th} = \Delta_0$ and $|\mu_b| = |\mu_t| = 5\Delta_0$.

of $\delta\rho(E,q)$ depends on both the energy E and the wavenumber q. However, one can clearly observe that for asymmetric doping $\delta\rho_t(E,q)$ has opposite sign to $\delta\rho_b(E,q)$. On the other hand, for symmetric doping $\delta\rho_t(E,q) = \delta\rho_b(E,q)$, which can be expected based on the inversion symmetry of the system. Since more than one AMSs gives contributions to $\delta\rho(E,q)$, these results cannot be directly related to individual broadening differences $\Gamma^e_{l,nn} - \Gamma^h_{l,nn}$, but they do illustrate the important effect of the doping of the two graphene layers. Furthermore, using the arguments put forward below equation (6), these results suggest that the sum of the $m = n$ terms in equation (7) gives a negative (positive) contribution to the differential conductance for asymmetric (symmetric) doping profile.

The contributions of the $m \neq n$ terms in equation (7) is more difficult to visualize, but our numerical calculations indicate that they give an equally important contribution to $G(eV)$. To illustrate this point, in figures 5(a) and (b) we show the q-resolved non-local differential conductance $G(eV,q)$ for asymmetric and symmetric doping, respectively, and weakly coupled normal leads N_1 and N_2. We used the same parameters as for the calculations in figure 4. The non-zero matrix elements of W_1 and W_2 are on the order $0.1\gamma_1$, where γ_1 is the interlayer coupling in Bernal stacked graphene. The general features in $G(eV,q)$ closely resemble the LDOS in figure 4, showing the important role of the AMSs in the non-local conductance for this relatively weak coupling between N_1, N_2 and the corresponding graphene layers. $G(eV,q)$ can be both positive and negative as a function of q, which indicates that the LDOS difference of the electron and hole quasiparticles, shown in figure 4, is not the only factor affecting it. However, as one can see by comparing figures 5(c) and (d), we find that the total non-local differential conductance $G(eV) = \sum_q G(eV,q)$ is mostly negative (positive) for asymmetric (symmetric) doping.

Next, we study the dependence of $G(eV)$ on the magnitude of the doping of the layers. In figure 6 we fixed the superconducting phase difference at $\varphi = 0$ and show the results for a setup with a large Thouless energy $E_{Th} = 3\Delta_0$. The white region around $eV = 0$, where $G(eV)$ vanishes, corresponds to $|eV| \leqslant \Delta_{ind}$. For low doping, when $\mu \lesssim 4\Delta_0$, the induced gap is almost the same as the bulk gap, i.e. $\Delta_{ind} \approx \Delta_0$ and $G(eV) \approx 0$. Δ_{ind} decreases as the doping is increased, and for energies $\Delta_{ind} \leqslant |eV| \leqslant \Delta_0$, CAR dominated differential conductance appears for the asymmetric doping case (figure 6(a)). In contrast, as shown in figure 6(b) for symmetric doping $G(eV)$ is usually positive, indicating EC dominated transport. We emphasize that contrary to the p-n junction setup suggested by [23], in our setup the doping of the graphene layers does not have to be smaller than Δ_0, which is experimentally difficult to achieve. The CAR dominated transport appears for dopings $\mu > \Delta_0$, when $\Delta_{ind} < \Delta_0$. We performed similar calculations as in figure 6(a) for longer junctions as well, see figures 7(a) and (b). We find extended regions of CAR dominated transport when the layers are asymmetrically doped and $\Delta_{ind} < \Delta_0$ is satisfied.

As mentioned previously, the superconducting phase difference φ can be another way to tune the non-local transport. Typically, the JJ where φ should be tuned is part of a large SQUID loop [50, 51]. The magnetic field used in e.g. [50] to change φ was of the order of 0.05 mT. Such low magnetic fields should have negligible orbital effects in the top and bottom graphene layers, therefore we do not include it

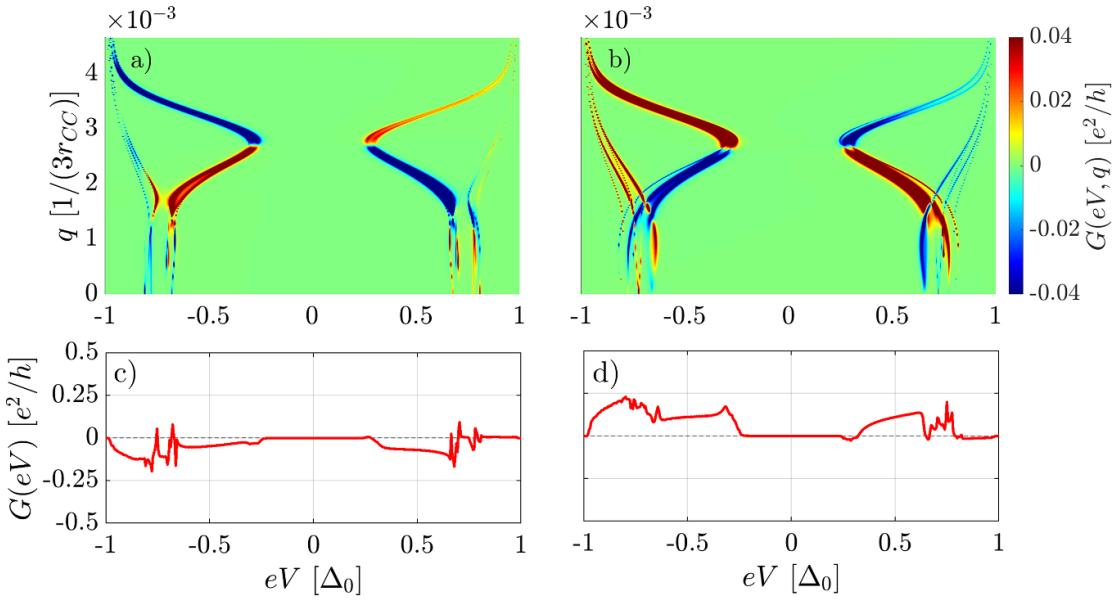

Figure 5. The q-resolved non-local differential conductance $G(eV, q)$ for (a) asymmetric and (b) symmetric doping for the systems shown in figure 4. (c) and (d) The total differential conductance $G(eV)$ corresponding to the case in (a) and (b), respectively.

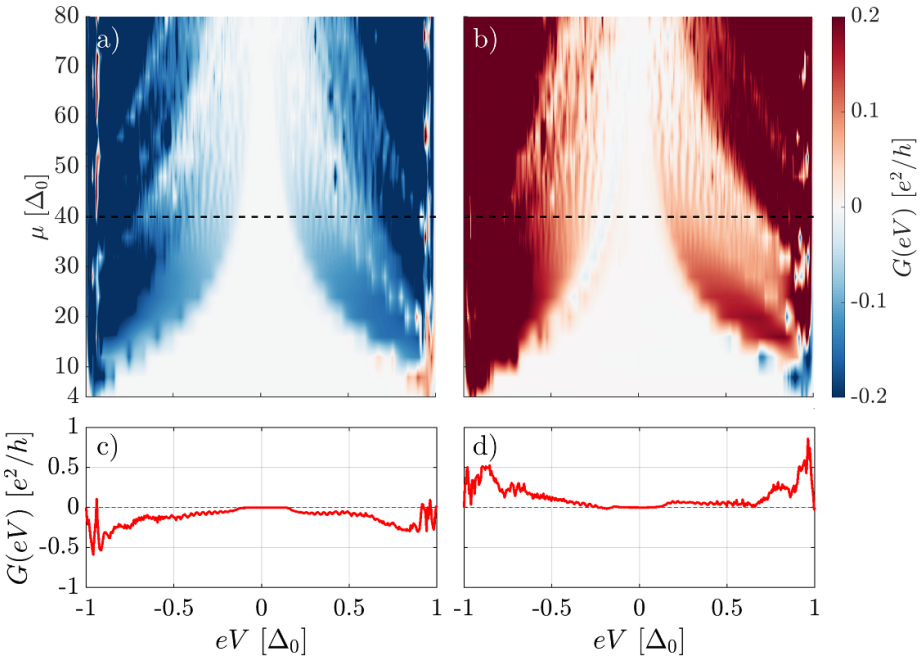

Figure 6. The non-local differential conductance $G(eV)$ as a function of the doping of the graphene layers μ and the applied voltage V, at superconducting phase difference $\varphi = 0$, and Thouless energy $E_{Th} = 3\Delta_0$. In (a) an asymmetric doping profile $\mu_b = -\mu_t = \mu$ is used, while in (b) the doping is symmetric $\mu_b = \mu_t = -\mu$. (c) and (d): $G(eV)$ trace along the dashed line at $\mu = 40\Delta_0$ in (a) and (b), respectively. Negative $G(eV)$ indicates CAR dominated transport.

explicitly, i.e. through a vector potential $\mathbf{A}(\mathbf{r})$, in the following calculations. We assume that the only relevant effect of the magnetic field is to change φ in the JJ.

We discuss the φ dependence of the differential conductance in the calculations shown in figure 8(a), where we used the same E_{Th} as in figure 6(a), whereas figure 8(b) corresponds to the case in figure 7(a). We remind that as φ increases from 0 to π, the induced gap in the graphene layers is gradually reduced and Δ_{ind} goes to zero for $\varphi = \pi$, see figures 2(d)–(f). This appears as a shrinking, low-conductance white region for $|eV| \lesssim \Delta_{ind}$ in figures 8(a) and (b). However, $G(eV)$ is finite and negative in the range $\Delta_{ind} \leqslant |eV| \leqslant \Delta_0$ for most values of φ, suggesting that CAR is also robust to the change of φ. Similar behavior can

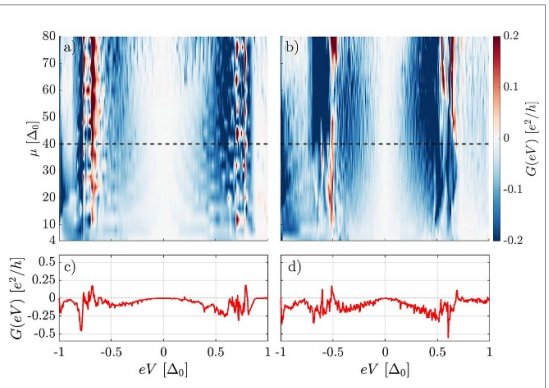

Figure 7. The non-local differential conductance $G(eV)$ as a function of the doping of the graphene layers μ for an asymmetric doping profile in the long junction regime. In (a) we used $E_{Th} = \Delta_0$ and in (b) $E_{Th} = 0.6\Delta_0$ and the legend for different colors is given in figure 6. The superconducting phase difference is $\varphi = 0$. (c) and (d): $G(eV)$ trace along the dashed line at $\mu = 40\Delta_0$ in (a) and (b), respectively.

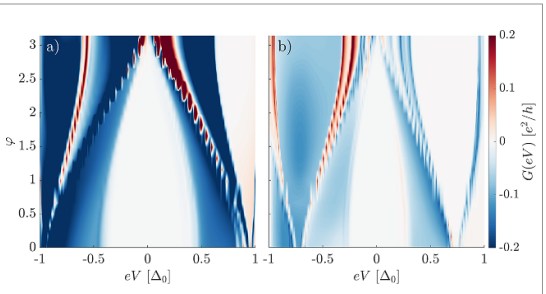

Figure 8. The differential conductance $G(eV)$ as a function of the superconducting phase difference φ, for (a) a device in the short junction regime, $E_{Th} = 3\Delta_0$ and doping $\mu_b = -\mu_t = 20\Delta_0$, and (b) $E_{Th} = \Delta_0$ and $\mu_b = -\mu_t = 5\Delta_0$. The legend for different colors is given in figure 6.

be seen for both $E_{Th} = 3\Delta_0$ and $E_{Th} = \Delta_0$. We have checked that for symmetric doping $\mu_t = \mu_b$ the differential conductance is mostly positive for all values of φ, i.e. the interlayer transport is dominated by EC.

5. Conclusion

In conclusion, we have studied non-local Andreev reflection in a monolayer graphene based double JJ geometry. We have shown, that the ABSs appearing in the graphene layers hybridize and form AMSs. By studying the non-local differential conductance, we found that choosing an asymmetric doping profile in the graphene layers leads to CAR dominated transport mediated by the AMSs. Changing the doping profile to a symmetric one leads to the suppression of CAR. Importantly, the observed negative differential conductance does not require a very low doping of the graphene layers, which is difficult to achieve. We found that the negative non-local differential conduction is robust with respect to the junction length, changes in the doping of the graphene layers and the superconducting phase difference.

Data availability statement

All data that support the findings of this study are included within the article (and any supplementary files).

Acknowledgments

This work was supported by the ÚNKP-22-5 New National Excellence Program of the Ministry for Innovation and Technology from the source of the National Research, Development and Innovation Fund and by the Hungarian Scientific Research Fund (OTKA) Grant No. K134437. A K and P R acknowledge support from the Hungarian Academy of Sciences through the Bólyai János Stipendium (BO/00603/20/11 and BO/00571/22/11) as well. The research was supported by the Ministry of Innovation and Technology and the National Research, Development and Innovation Office within the Quantum Information National Laboratory of Hungary and we acknowledge the computational resources provided by the Wigner Scientific Computational Laboratory (WSCLAB).

ORCID iD

Andor Kormányos https://orcid.org/0000-0002-6837-6966

References

[1] Vidal G 2003 Efficient classical simulation of slightly entangled quantum computations *Phys. Rev. Lett.* **91** 147902
[2] Recher P, Sukhorukov E V and Loss D 2001 Andreev tunneling, Coulomb blockade, and resonant transport of nonlocal spin-entangled electrons *Phys. Rev.* B **63** 165314
[3] Lesovik G, Martin T and Blatter G 2001 Electronic entanglement in the vicinity of a superconductor *Eur. Phys. J.* B **24** 287–90
[4] Samuelsson P, Sukhorukov E V and Büttiker M 2003 Orbital entanglement and violation of bell inequalities in mesoscopic conductors *Phys. Rev. Lett.* **91** 157002
[5] Prada E and Sols F 2004 Entangled electron current through finite size normal-superconductor tunneling structures *Eur. Phys. J.* B **40** 379
[6] Beckmann D, Weber H B and v. Löhneysen H 2004 Evidence for crossed Andreev reflection in superconductor ferromagnet hybrid structures *Phys. Rev. Lett.* **93** 197003
[7] Russo S, Kroug M, Klapwijk T M and Morpurgo A F 2005 Morpurgo, Experimental observation of bias-dependent nonlocal Andreev reflection *Phys. Rev. Lett.* **95** 027002
[8] Hofstetter L, Csonka S, Nygård J and Schönenberger C 2009 Cooper pair splitter realized in a two-quantum-dot Y-junction *Nature* **461** 960
[9] Hofstetter L, Csonka S, Baumgartner A, Fülöp G, d'Hollosy S, Nygård J and Schönenberger C 2011 Finite bias Cooper pair splitting *Phys. Rev. Lett.* **107** 136801
[10] Das A, Ronen Y, Heiblum M, Mahalu D, Kretinin A V and Shtrikman H 2012 High-efficiency Cooper pair splitting demonstrated by two-particle conductance resonance and positive noise cross-correlation *Nat. Commun.* **3** 1165
[11] Ueda K *et al* 2019 Dominant nonlocal superconducting proximity effect due to electron-electron interaction in a ballistic double nanowire *Sci. Adv.* **5** eaaw2194

[12] Kürtössy O, Scherübl Z, Fülöp G, Lukács I E, Kanne T, Nygård J, Makk P and Csonka S 2022 Parallel InAs nanowires for cooper pair splitters with coulomb repulsion (arXiv:2203.14397)
[13] Wang G *et al* 2022 Singlet and triplet Cooper pair splitting in superconducting-semiconducting hybrid nanowires (arXiv:2205.03458)
[14] Herrmann L G, Portier F, Roche P, Yeyati A L, Kontos T and Strunk C 2010 Carbon nanotubes as Cooper pair beam splitters *Phys. Rev. Lett.* **104** 026801
[15] Schindele J, Baumgartner A and Schönenberger C 2012 Near-unity Cooper pair splitting efficiency *Phys. Rev. Lett.* **109** 157002
[16] Brange F, Prech K and Flindt C 2021 Dynamic Cooper pair splitter *Phys. Rev. Lett.* **127** 237701
[17] Tan Z B, Cox D, Nieminen T, Lähteenmäki P, Golubev D, Lesovik G B and Hakonen P J 2015 Cooper pair splitting by means of graphene quantum dots *Phys. Rev. Lett.* **114** 096602
[18] Borzenets I, Shimazaki Y, Jones G, Craciun M, Russo S, Yamamoto Y and Tarucha S 2015 High efficiency CVD graphene-lead (Pb) Cooper pair splitter *Sci. Rep.* **6** 23051
[19] Pöschl A, Danilenko A, Sabonis D, Kristjuhan K, Lindemann T, Thomas C, Manfra M J and Marcus C M 2022 Nonlocal conductance spectroscopy of Andreev bound states in gate-defined InAs/Al nanowires (arXiv:2204.02430)
[20] Falci G, Feinberg D and Hekking F W 2001 Correlated tunneling into a superconductor in a multiprobe hybrid structure *Europhys. Lett.* **54** 255
[21] Walldorf N, Brange F, Padurariu C and Flindt C 2020 Noise and full counting statistics of a Cooper pair splitter *Phys. Rev.* B **101** 205422
[22] Liu C-X, Wang G, Dvir T and Wimmer M 2022 Tunable Superconducting Coupling of Quantum Dots via Andreev Bound States in Semiconductor-Superconductor Nanowires *Phys. Rev. Lett.* 129 267701
[23] Cayssol J 2008 Crossed Andreev reflection in a graphene bipolar transistor *Phys. Rev. Lett.* **100** 147001
[24] Veldhorst M and Brinkman A 2010 Nonlocal cooper pair splitting in a *p***S***n* junction *Phys. Rev. Lett.* **105** 107002
[25] Xue J, Sanchez-Yamagishi J, Bulmash D, Jacquod P, Deshpande A, Watanabe K, Taniguchi T, Jarillo-Herrero P and LeRoy B J 2011 Scanning tunnelling microscopy and spectroscopy of ultra-flat graphene on hexagonal boron nitride *Nat. Mater.* **10** 282
[26] Mayorov A S, Elias D C, Mukhin I S, Morozov S V, Ponomarenko L A, Novoselov K S, Geim A K and Gorbachev R V 2012 How close can one approach the Dirac point in graphene experimentally? *Nano Lett.* **12** 4629
[27] Park G-H, Watanabe K, Taniguchi T, Lee G-H and Lee H-J 2019 Engineering crossed Andreev reflection in double-bilayer graphene *Nano Lett.* **19** 9002
[28] Efetov D K *et al* 2016 Specular interband Andreev reflections at van der Waals interfaces between graphene and $NbSe_2$ *Nat. Phys.* **12** 328
[29] Pandey P, Danneau R and Beckmann D 2021 Ballistic graphene Cooper pair splitter *Phys. Rev. Lett.* **126** 147701
[30] Soori A and Mukerjee S 2017 Enhancement of crossed andreev reflection in a superconducting ladder connected to normal metal leads *Phys. Rev.* B **95** 104517
[31] Nehra R, Bhakuni D S, Sharma A and Soori A 2019 Enhancement of crossed andreev reflection in a kitaev ladder connected to normal metal leads *J. Phys.: Condens. Matter* **31** 345304
[32] Pillet J-D, Benzoni V, Griesmar J, Smirr J-L and Girit C O 2019 Nonlocal Josephson effect in Andreev molecules *Nano Lett.* **19** 7138
[33] Kornich V, Barakov H S and Nazarov Y V 2019 Fine energy splitting of overlapping Andreev bound states in multiterminal superconducting nanostructures *Phys. Rev. Res.* **1** 033004
[34] Indolese D I, Karnatak P, Kononov A, Delagrange R, Haller R, Wang L, Makk P, Watanabe K, Taniguchi T and Schönenberger C 2020 Compact SQUID realized in a double-layer graphene heterostructure *Nano Lett.* **20** 7129
[35] Bretheau L, Wang J I-J, Pisoni R, Watanabe K, Taniguchi T and Jarillo-Herrero P 2017 Tunnelling spectroscopy of Andreev states in graphene *Nat. Phys.* **13** 756
[36] Titov M and Beenakker C W 2006 Josephson effect in ballistic graphene *Phys. Rev.* B **74** 041401(R)
[37] Tworzydło J, Trauzettel B, Titov M, Rycerz A and Beenakker C W J 2006 Sub-poissonian shot noise in graphene *Phys. Rev. Lett.* **96** 246802
[38] Titov M and Beenakker C W J 2006 Josephson effect in ballistic graphene *Phys. Rev.* B **74** 041401
[39] Rakyta P 2015 Eötvös Quantum utilities (available: http://eqt.elte.hu/EQuUs/html/)
[40] Titov M, Ossipov A and Beenakker C W 2007 Excitation gap of a graphene channel with superconducting boundaries *Phys. Rev.* B **75** 045417
[41] Manjarrés D A, Gomez S and Herrera W J 2014 Andreev levels in a Andreev superconductor graphene superconductor nanostructure *Physica* B **455** 26
[42] Ben Shalom M *et al* 2016 Quantum oscillations of the critical current and high-field superconducting proximity in ballistic graphene *Nat. Phys.* **12** 318
[43] Banszerus L, Libisch F, Ceruti A, Blien S, Watanabe K, Taniguchi T, Hüttel A K, Beschoten B, Hassler F and Stampfer C 2020 Minigap and Andreev bound states in ballistic graphene (arXiv:2011.11471)
[44] Cresti A, Farchioni R, Grosso G and Parravicini G P 2003 Keldysh-Green function formalism for current profiles in mesoscopic systems *Phys. Rev.* B **68** 075306
[45] Do V N 2014 Non-equilibrium Green function method: theory and application in simulation of nanometer electronic devices *Adv. Nat. Sci.: Nanosci. Nanotechnol.* **5** 033001
[46] Pala M G, Governale M and König J 2008 Nonequilibrium Josephson and Andreev current through interacting quantum dots *New J. Phys.* **10** 099801
[47] Bolech C J and Giamarchi T 2005 Keldysh study of pointcontact tunneling between superconductors *Phys. Rev.* B **71** 024517
[48] Wu S-T and Yip S 2004 ac Josephson effect in asymmetric superconducting quantum point contacts *Phys. Rev.* B **70** 104511
[49] Claughton N R, Leadbeater M and Lambert C J 1995 Theory of Andreev resonances in quantum dots *J. Phys.: Condens. Matter* **7** 8757
[50] Nanda G, Aguilera-Servin J L, Rakyta P, Kormá nyos A, Kleiner R, Koelle D, Watanabe K, Taniguchi T, Vandersypen L M K and Goswami S 2017 Current-phase relation of ballistic graphene Josephson junctions *Nano Lett.* **17** 3396
[51] Della Rocca M L, Chauvin M, Huard B, Pothier H, Esteve D and Urbina C 2007 Measurement of the currentphase relation of superconducting atomic contacts *Phys. Rev. Lett.* **99** 127005